Title: Real-time imaging of DNA loop extrusion by condensin

Authors: Mahipal Ganji,[1] Indra A. Shaltiel,[2]* Shveta Bisht,[2]* Eugene Kim,[1] Ana Kalichava,[1] Christian H. Haering,[2]† Cees Dekker[1]†

Affiliations:

[1]Department of Bionanoscience, Kavli Institute of Nanoscience Delft, Delft University of Technology, Delft, Netherlands.

[2]Cell Biology and Biophysics Unit, Structural and Computational Biology Unit, European Molecular Biology Laboratory (EMBL), Heidelberg, Germany.

*These authors contributed equally to this work.
†Corresponding authors. Email: christian.haering@embl.de; c.dekker@tudelft.nl

Abstract:

Structural Maintenance of Chromosomes (SMC) protein complexes, including condensin and cohesin, are central actors in the spatial organization of chromosomes in all species. It has been hypothesized that these ring-shaped complexes organize chromosomes by extruding DNA through their central opening to create large DNA loops. Here, we provide unambiguous evidence for such loop extrusion by directly visualizing the formation and processive extension of DNA loops by *Saccharomyces cerevisiae* condensin in real-time movies. We find that condensin is able to extrude DNA loops as large as 40 kilobase pairs (the physical upper limit in our assay) at a strongly force-dependent rate of up to 1,500 base pairs per second. Dual-color imaging of condensin and DNA reveals that loop extrusion is driven by condensin at the stem of the extruded DNA loop. Condensin-induced loop extrusion requires ATP hydrolysis and is strictly asymmetric, which suggests that condensin anchors onto DNA and reels it in from only one side. DNA loop extrusion by SMC complexes may hence provide the universal unifying principle for genome organization.

One Sentence Summary:

Single-molecule imaging reveals the ATP-hydrolysis-dependent formation of large DNA loops by condensin complexes, providing direct evidence for a loop-extrusion mechanism as the basic organizational principle of chromosome structure.

Main Text:

The spatial organization of chromosomes is of paramount importance to cell biology. Members of the SMC family of protein complexes, including condensin, cohesin, and the Smc5–Smc6 complex, play vital roles in restructuring genomes during the cellular life cycle (*1-3*). Whereas cohesin is important for gene regulation, DNA damage repair, and holding together sister chromatids (*4*), condensin is essential for the formation of compact mitotic chromosomes and the resolution of sister chromatids in preparation for cell division (*5*).

The principles by which SMC complexes achieve these fundamental tasks are still poorly understood and subject of intense debate. Models based on random cross-linking of DNA strands by pairwise interactions or conformational changes in the superhelicity of the DNA helix have been proposed for SMC-driven DNA organization (*5, 6*). An alternative hypothesis suggests that SMC protein complexes create and subsequently extrude DNA loops (*4*), which would elegantly explain features of mitotic chromosomes observed in electron micrographs and deduced from Hi-C chromosome conformation capture experiments (*7, 8*). Indeed, recent polymer simulations showed that loop extrusion can, in principle, result in the efficient disentanglement and compaction of chromatin fibers (*9-11*). The recent discovery that condensin exhibits DNA translocase activity (*12*) is consistent with, but does not provide conclusive evidence for (*13*), the extrusion of DNA loops by condensin.

In this study, we set out to visualize the formation of DNA loops by the *S. cerevisiae* condensin complex (Fig. 1A) (*14*). We tethered both ends of a double-stranded 48.5-kilobase pair (kbp) λ-DNA molecule to a passivated surface in a microfluidic chamber (*15, 16*), adjusting the end-to-end DNA length by the flow such that the tethered DNA was only slightly stretched to a distance much shorter than its contour length (Fig. 1B). We visualized the DNA by Sytox Orange (SxO) staining in a fluorescence microscope. As expected, the SxO fluorescence intensity was homogenously distributed along the length of the double-tethered DNA molecule (Fig. 1C and Movie S1). When we subsequently flushed in 1 nM of purified condensin (*12, 17*) and 5 mM of ATP in an imaging buffer (see Methods), we observed the accumulation of fluorescence density at a random position along the length of the DNA. This finding shows that condensin induces local compaction of DNA (Fig. 1D, E and Movie S2).

To visualize the compacted DNA structures in the imaging plane of the microscope, we applied a fluid flow at a large angle with respect to the double-tethered DNA. This revealed that the bright spots were in fact made up of long-extended pieces of DNA, consistent with single large DNA loops (Fig. 1F, G, Fig. S1 and Movie S3). Importantly, the formation of DNA loops only occurred in the presence of wild-type condensin and ATP. A mutant version of condensin that is unable to bind and hydrolyze ATP due to mutations in the Q-loop motifs of Smc2 and Smc4 did not produce any local increase in DNA density (see below). We also observed no DNA loop formation by wild-type condensin in the absence of either ATP or Mg^{2+}. These observations show that condensin creates DNA loops in an ATP-hydrolysis-dependent manner, either by gradually extruding DNA or by randomly grabbing and linking two different spots on the DNA.

To distinguish between these two possibilities, we monitored the looping process in real time. We achieved this by applying, from the start, a constant flow perpendicular to the immobilized DNA, while continuously imaging the SxO-stained DNA in the imaging plane. Time-lapse imaging revealed the appearance of an initially weak increase in fluorescence intensity at a local spot that grew into an extended loop over time (Fig. 2A, Fig. S2, and Movies S4-S5). The continuous growth

of an extended DNA structure provides direct visual proof of loop-extrusion activity, and rules out the alternative model of random cross-linking of two DNA sites, which would instead have shown the sudden appearance of a bright fluorescent structure that would have remained stable in size over time. The loop extrusion process in the example of figure 2A occurred over the course of about 1 minute. The loop structure then remained stable for about 10 minutes, after which the extruded loop disrupted in a single step, resulting in the return of a homogenous DNA intensity that was identical to the bare DNA at the start of the experiment (see last panel in Fig. 2A and Movies S6-S7). Such a single-step disruption behavior suggests that the DNA loop had been extruded from a single condensin unit, composed of one or multiple condensin complexes, which spontaneously let go of the DNA or disassembled from it. If the loop had been formed by many condensin units at the stem or distributed along the length of the loop, one would have expected a more gradual, multi-step relaxation of the loop instead of the observed single-step release.

Higher temporal resolution imaging allowed us to resolve the two individual DNA strands in the extruded loop in consecutive time frames, which showed that an actual loop had been extruded rather than an intertwined or otherwise connected structure (Fig. 2B, Fig. S3 and Movie S8).

To quantify the kinetics of loop extrusion, we returned to imaging in the absence of flow. Figure 3A shows an example where the loop first nucleated as a single weak fluorescent spot that subsequently expanded in size over time due to loop extrusion (Fig. 3A and Movies S9 and S10). We constructed a kymograph from these data by integrating the fluorescence intensity along the length of the DNA in each frame (Fig. 3B and Methods) and divided each line of the kymograph into three regions based on the position of the loop: the DNA from the top attachment point up to the base of the loop (I, orange), the DNA loop itself (II, red), and the DNA between the loop and the bottom attachment point (III, cyan) (Fig. 3C). We then calculated the DNA lengths in each region from the fluorescence intensities and the known 48.5-kbp length of the λ-DNA.

This revealed the extrusion of >20 kbp DNA in ~20 seconds in the example of Fig. 3C, before reaching a plateau (region II). Simultaneously, the DNA content of the bottom part of the DNA (region III) decreased by the same amount, whereas the DNA content of the top part of the DNA (region I) did *not* change at all during the loop extrusion process. This result strikingly demonstrates that the loop extrusion process is asymmetric – contrary to what has been commonly hypothesized (*9, 10*). Additional examples for asymmetric loop extrusion on DNA molecules with different end-to-end attachment lengths are shown in figures 3D and 3E. For all individual loop extrusion events that we analyzed quantitatively (N=14), we consistently observed the same characteristic features: an increase in loop size until reaching a plateau (Fig. 3F), a concomitant decrease in the length of DNA ahead of loop (Fig. 3G), and a constant size of DNA behind the loop (Fig. 3H). These features robustly demonstrate the asymmetric nature of loop extrusion by condensin.

We can estimate the speed of loop extrusion from the slopes of the linear part of the curves in figure 3G, which yields a DNA loop-extrusion rate of 0.98 ± 0.42 kbp/s (mean ± SD, Fig. 3I). While this number is significantly higher than previous *in vitro* estimates from single-molecule experiments with *S. cerevisiae* condensin (*12, 17*), it matches well the condensation rates of 0.7 kbp/s reported for condensin II in chicken DT40 cells (*18*), 0.9 kbp/s for the SMC complex in *Bacillus subtilis* (*19*), and 1 kbp/s for condensin I purified from *Xenopus laevis* egg extracts (*20*). We note that our assay provides a very clean and indisputable measurement of the condensation rate, since it avoids any discussions about roadblocks, multiple condensin units working in series or in parallel at different positions on the DNA, etc.

Analysis of the rate of loop extrusion from individual DNA molecules and their corresponding end-to-end lengths shows that the speed of loop extrusion by condensin strongly depends on the relative extension of the DNA (Fig. 3J), which also explains the large standard deviation in loop extrusion rates in figure 3I. Interestingly, we observed extrusion rates as high as 1,500 kbp/s at low DNA extensions. The dependence of the extrusion rate on the DNA end-to-end length can be understood as a force dependence: As the loop is extruded, the amount of DNA between the two attachment points (excluding the loop size) decreases correspondingly, thus continuously increasing the force within the DNA molecule (*12, 21*). This can lead to such high force values (1.4 ± 0.5 pN; N=6) (*15*) that the extrusion process stalls, as is for example seen in figure 3D. Accordingly, we can use the known force-extension relation to plot the loop extrusion rate versus force (Fig. 3K, Fig. S4 and Methods), which reveals a strikingly steep dependence on force. This very strong force dependence, where the loop extrusion rate drops significantly near 0.4 pN, indicates that condensin is a fast yet weak loop-extruding motor that rapidly stalls against any modest force applied to the DNA. The dependence on force furthermore explains why our measured rate of loop extrusion is about 20 times faster than the motor speed measured in DNA curtains assays (*12*), as the loop extrusion rate extrapolates to similar values for the large relative DNA extension of ~0.75 used in the curtains assay (cf. Fig. 3J).

Biochemical analysis indicated that the ATP hydrolysis rate for the condensin complex used in our study is about 4 molecules per second in the presence of DNA (Fig. S5E). Importantly, one should note that such a bulk estimate only provides a lower limit of the ATPase activity of condensin complexes that are in the active process of loop extrusion, since non-DNA-bound condensin molecules and complexes that have stalled on the DNA are included in these assays. Nevertheless, if we assume, for the sake of argument, that condensin extrudes ~1 kbp/s of DNA while hydrolyzing 4 molecules of ATP, it might take steps of length that are of the order of the size of a single condensin complex. There are multiple scenarios to explain such large steps (*12, 22, 23*), including ones where steps depend on the flexibility of DNA such that, at low forces, condensin can reach nearby spots on the folded DNA structure to occasionally capture and extrude pieces of DNA much longer than the condensin size itself – a scenario that would be consistent with the very strong force dependence of the extrusion rate that we observe.

Finally, we co-visualized condensin acting on the extruded DNA loop. For the simultaneous visualization of SxO-labelled DNA and condensin in the act of loop extrusion, we labeled purified condensin holocomplexes with a single ATTO647N fluorophore (Fig. S5). We co-imaged the SxO-labelled DNA in epi-fluorescence mode and the ATTO647N-labelled condensin in total internal reflection fluorescence (TIRF) mode by alternating the excitation modes (see Methods). Figure 4 shows an example where, as expected, condensin localizes to the stem of the extruded DNA loop (Movie S11). Interestingly, upon appearance of ATTO647N fluorescence on the DNA in a single step, a loop immediately started to appear on the DNA (Fig. S6), which is consistent with the notion that DNA loops are extruded by a single condensin unit.

SMC complexes are vital for chromosome organization in all domains of life. However, the molecular basis for their action so far remained largely speculative. Our experiments, for the first time, unambiguously demonstrate that condensin exhibits a DNA loop-extrusion activity. Our real-time single-molecule dual-color movies of condensin and DNA reveal that loops are extruded by condensin at stem of the loop in a manner that is ATP hydrolysis-dependent, strictly asymmetric and highly sensitive to forces applied to the DNA. These properties can be explained by a model (Fig. 4C) where condensin is able to stably hold on to a position in the DNA, possibly through a

direct DNA binding site formed by its Brn1 and Ycg1 subunits (*24*), and then reel in DNA from only one side while maintaining a stable contact with the original binding site. The visual proof that condensin is a loop-extruding enzyme provides the key principle that underlies the organization of genome architecture by condensin and most likely all other SMC protein complexes.

References and Notes:

1. L. Aragon, E. Martinez-Perez, M. Merkenschlager, Condensin, cohesin and the control of chromatin states. *Current Opinion in Genetics & Development* **23**, 204 (2013).
2. F. Uhlmann, SMC complexes: from DNA to chromosomes. *Nature Reviews Molecular Cell Biology* **17**, 399 (2016).
3. K. Jeppsson, T. Kanno, K. Shirahige, C. Sjogren, The maintenance of chromosome structure: positioning and functioning of SMC complexes. *Nature reviews. Molecular cell biology* **15**, 601 (2014).
4. K. Nasmyth, Disseminating the Genome: Joining, Resolving, and Separating Sister Chromatids During Mitosis and Meiosis. *Annual Review of Genetics* **35**, 673 (2001).
5. T. Hirano, Condensin-Based Chromosome Organization from Bacteria to Vertebrates. *Cell* **164**, 847 (2012).
6. R. Thadani, F. Uhlmann, S. Heeger, Condensin, Chromatin Crossbarring and Chromosome Condensation. *Current Biology* **22**, R1012 (2012).
7. J. R. Paulson, U. K. Laemmli, The structure of histone-depleted metaphase chromosomes. *Cell* **12**, 817 (1977).
8. N. Naumova *et al.*, Organization of the Mitotic Chromosome. *Science* **342**, 948 (2013).
9. A. Goloborodko, M. V. Imakaev, J. F. Marko, L. Mirny, Compaction and segregation of sister chromatids via active loop extrusion. *eLife* **5**, e14864 (2016).
10. E. Alipour, J. F. Marko, Self-organization of domain structures by DNA-loop-extruding enzymes. *Nucleic Acids Research* **40**, 11202 (2012).
11. A. Goloborodko, John F. Marko, Leonid A. Mirny, Chromosome Compaction by Active Loop Extrusion. *Biophysical Journal* **110**, 2162 (2016).
12. T. Terakawa *et al.*, The condensin complex is a mechanochemical motor that translocates along DNA. *Science* **358**, 672 (2017).
13. K. Nasmyth, How are DNAs woven into chromosomes? *Science* **358**, 589 (2017).
14. J. Eeftens, C. Dekker, Catching DNA with hoops—biophysical approaches to clarify the mechanism of SMC proteins. *Nature Structural &Amp; Molecular Biology* **24**, 1012 (2017).
15. M. Ganji, S. H. Kim, J. van der Torre, E. Abbondanzieri, C. Dekker, Intercalation-Based Single-Molecule Fluorescence Assay To Study DNA Supercoil Dynamics. *Nano letters* **16**, 4699 (2016).
16. S. H. Kim, M. Ganji, J. v. d. Torre, E. Abbondanzieri, C. Dekker, DNA sequence encodes the position of DNA supercoils. *bioRxiv* (2017).

17. J. M. Eeftens *et al.*, Real-time detection of condensin-driven DNA compaction reveals a multistep binding mechanism. *The EMBO Journal* **36**, 3448 (2017).

18. J. H. Gibcus *et al.*, Mitotic chromosomes fold by condensin-dependent helical winding of chromatin loop arrays. *bioRxiv* (2017).

19. X. Wang, H. B. Brandão, T. B. K. Le, M. T. Laub, D. Z. Rudner, Bacillus SMC complexes juxtapose chromosome arms as they travel from origin to terminus. *Science* **355**, 524 (2017).

20. T. R. Strick, T. Kawaguchi, T. Hirano, Real-time detection of single-molecule DNA compaction by condensin I. *Current biology : CB* **14**, 874 (2004).

21. C. Bustamante, S. B. Smith, J. Liphardt, D. Smith, Single-molecule studies of DNA mechanics. *Current Opinion in Structural Biology* **10**, 279 (2000).

22. J. Lawrimore, B. Friedman, A. Doshi, K. Bloom, RotoStep: A Chromosome Dynamics Simulator Reveals Mechanisms of Loop Extrusion. *Cold Spring Harbor Symposia on Quantitative Biology*, 033696 (2017).

23. M.-L. Diebold-Durand *et al.*, Structure of Full-Length SMC and Rearrangements Required for Chromosome Organization. *Molecular Cell* **67**, 334 (2017).

24. M. Kschonsak *et al.*, Structural Basis for a Safety-Belt Mechanism That Anchors Condensin to Chromosomes. *Cell* **171**, 588 (2016).

25. J. Yin, A. J. Lin, D. E. Golan, C. T. Walsh, Site-specific protein labeling by Sfp phosphopantetheinyl transferase. *Nature protocols* **1**, 280 (2006).

26. J. Yin *et al.*, Genetically encoded short peptide tag for versatile protein labeling by Sfp phosphopantetheinyl transferase. *Proceedings of the National Academy of Sciences of the United States of America* **102**, 15815 (2005).

27. M. Ganji, M. Docter, S. F. J. Le Grice, E. A. Abbondanzieri, DNA binding proteins explore multiple local configurations during docking via rapid rebinding. *Nucleic Acids Research* **44**, 8376 (2016).

Acknowledgments:

We acknowledge Jaco van der Torre and Jacob Kerssemakers for technical support and Allard Katan, Je-Kyung Ryu, Jorine Eeftens, and Eli van der Sluis for discussions. The work was supported by the ERC Advanced Grant SynDiv (grant number 669598 to C.D.) the ERC Consolidator Grant CondStruct (grant number 681365 to C.H.H.), the Netherlands Organization for Scientific Research (NWO/OCW) as part of the Frontiers of Nanoscience program (to C.D.) and a Rubicon Grant (to I.A.S.), and the European Molecular Biology Laboratory (EMBL).

Figures

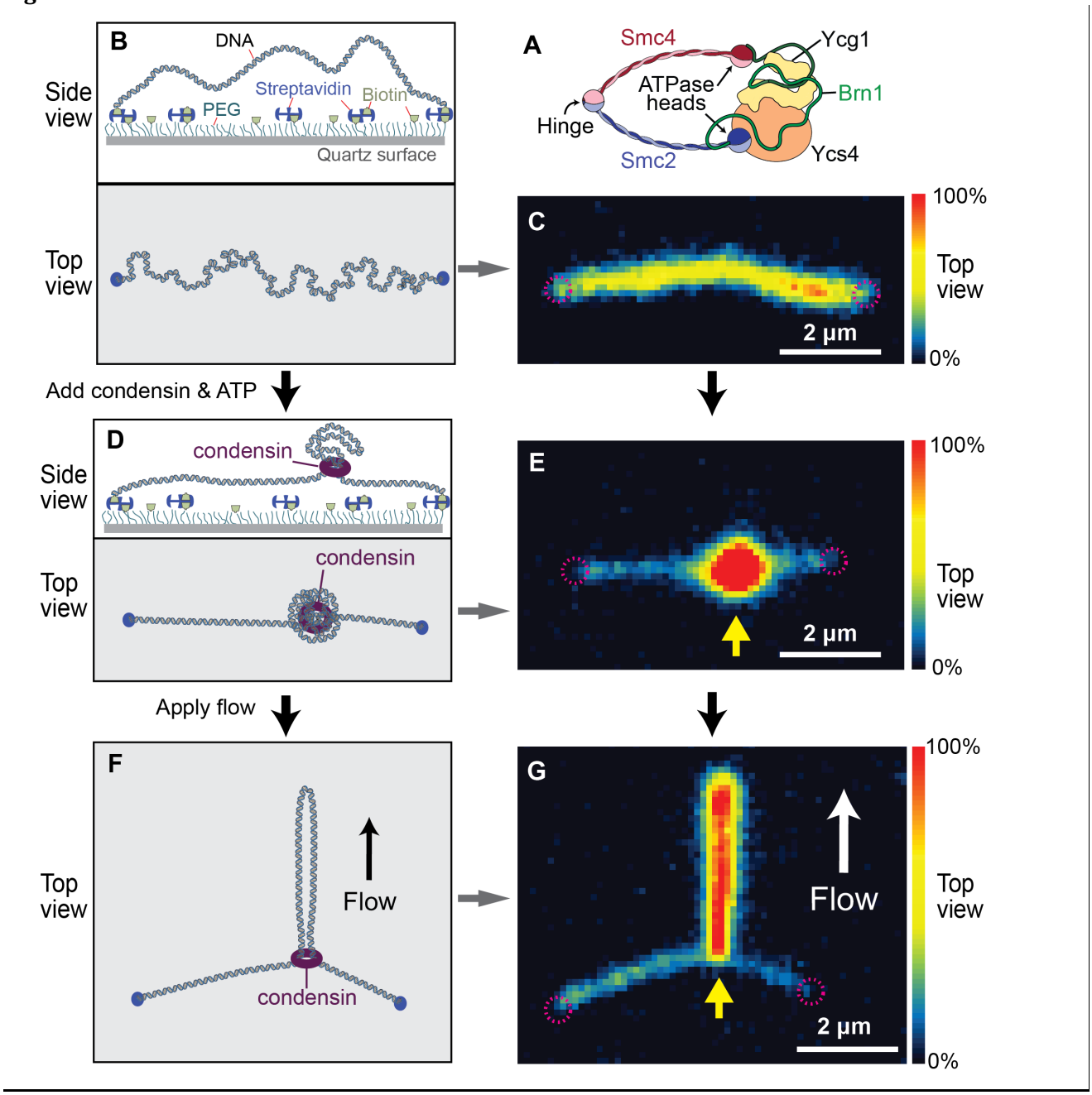

Fig. 1: Single-molecule assay for the visualization of condensin-mediated DNA looping. (**A**) Cartoon representation of the *S. cerevisiae* condensin complex. (**B**) Side and top view schematics of DNA that is doubly tethered to a PEG-passivated quartz surface via streptavidin-biotin linkage. (**C**) Snap-shot of a double-tethered λ-DNA molecule (100 ms exposure) visualized by Sytox Orange (SxO) staining. Dashed magenta circles indicate the surface attachment sites of the DNA. (**D**) Side and top view diagrams showing DNA loop formation on double-tethered DNA by condensin (purple). (**E**) Snap-shot of condensin-mediated DNA loop formation at one spot (indicated by the yellow arrow) along a SxO-stained DNA molecule. (**F**) Strategy to visualize DNA loops. Application of flow perpendicular to the axis of the immobilized DNA extends the loop within the imaging plane. (**G**) Snap-shot of an extended DNA loop that is stretched out by application of flow (white arrow) perpendicular to the DNA, as illustrated in (F).

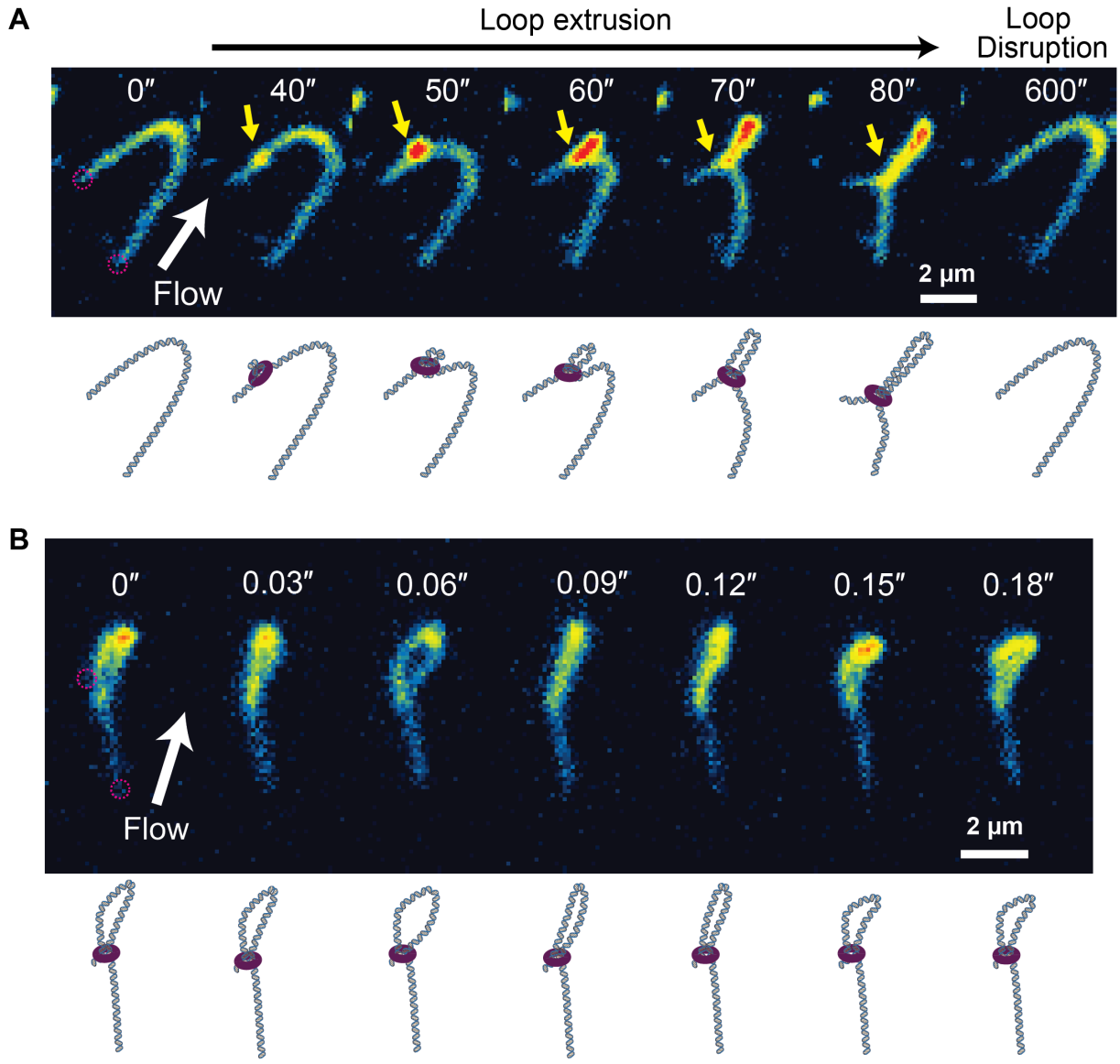

Fig. 2: Real-time imaging of DNA loop extrusion by condensin. (A) Series of snap-shots showing DNA loop extrusion intermediates created by condensin on a SxO-stained double-tethered λ-DNA (Movie S3). A constant flow was applied at a large angle with respect to the DNA axis (white arrow) which maintains the DNA in the imaging plane and stretches the extruded loop for visualization. The position of the loop base is indicated by a yellow arrow. At ~40 seconds, a small loop appears that grows over time until the majority of the DNA is contained in the loop at ~80 s. After ~600 s the loop suddenly disrupted, which made the DNA return to the initial loop-less configuration. Schematic diagrams under each snap-shot are for visual guidance. (**B**) High-time-resolution visualization displaying transient splitting of the two DNA strands in the extruded loop in adjacent time frames (cf. Movie S7). Time of each snap-shot is indicated in seconds.

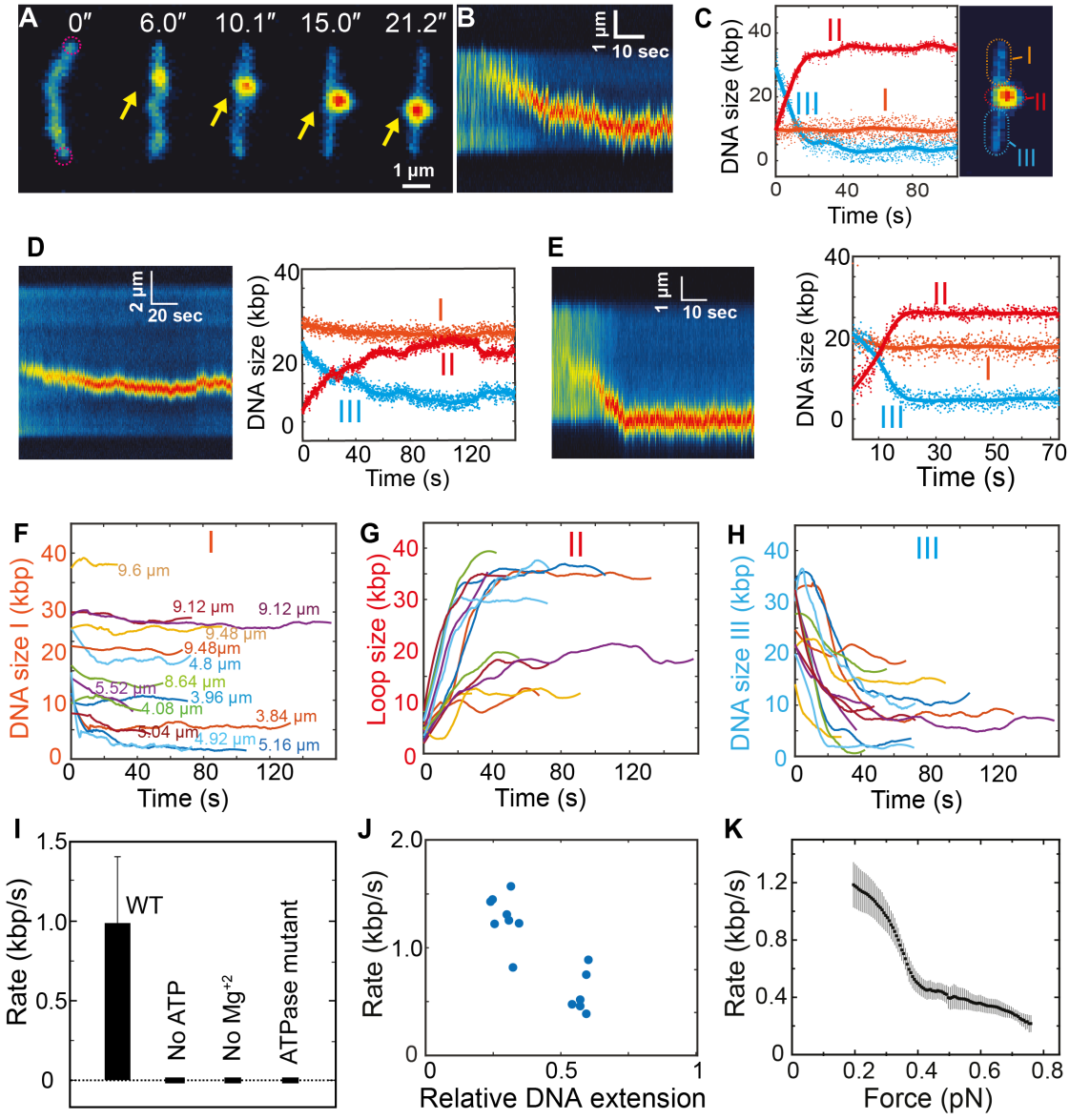

Fig. 3: Loop extrusion is asymmetric and depends on ATP hydrolysis. (**A**) Snap-shots showing the gradual extension of a DNA loop (yellow arrow) on a double-tethered λ-DNA molecule. No side flow is applied. (**B**) Kymograph of SxO fluorescence intensities shown in (A). (**C**) Time dependence of integrated DNA fluorescence intensities in the kymograph of panel (B) for 3 regions (see the right panel): (I; orange) DNA behind the loop, (II; red) the extruded loop, and (III; cyan) DNA ahead of the loop. (**D**) Kymograph and intensity plots of a more strongly stretched (9.12µm) DNA molecule that shows stalling of the loop extrusion somewhere midway along the length of DNA. (**E**) Kymograph and intensity plots of a DNA loop that starts in the middle of a stretched DNA and migrates until it reaches the physical barrier at the attachment site. (**F**), (**G**), and (**H**) Plots showing the lengths of the DNA behind (I), within (II), or ahead of (III) the DNA loop over time for individual molecules (N=14) of varying end-to-end length as indicated in the corresponding color in panel (F). (**I**) Bar plot showing the average rate of loop extrusion extracted from the linear rise in panel G (mean±SD). (**J**) Rate of loop extrusion versus the relative DNA extension compared with its 20 µm contour length. (**K**) Rate of loop extrusion versus the force that is exerted within the DNA due to the increased DNA stretching upon increasing the loop size by condensin.

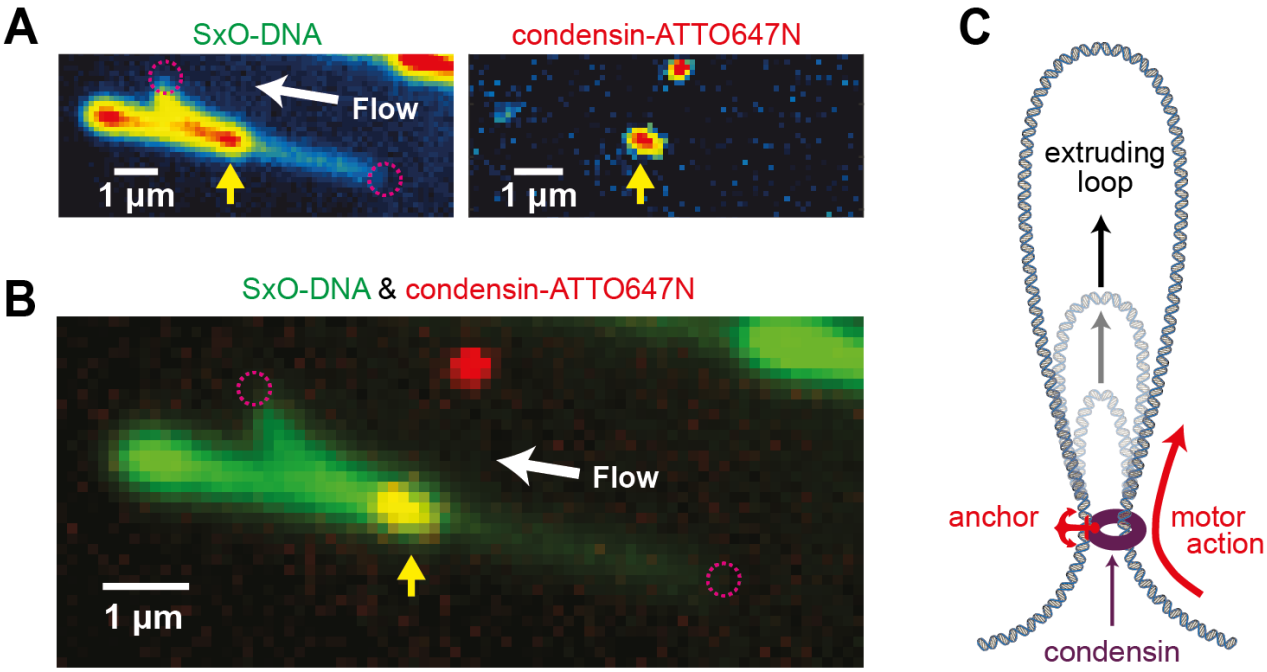

Fig. 4: Condensin is observed at the stem of the DNA loop during extrusion. (**A**) Left: fluorescence image of SxO-stained DNA exhibiting an extruded loop. Right: the exact same field of view as in the left side showing an ATTO647N-labelled condensin located at the stem of loop. Yellow arrows indicate the position of condensin at the stem of the DNA loop. All images in this figure are averages of movie frames taken over 2 s. (**B**) Overlaid images from panel A. DNA is shown in green and condensin in red. The arrow indicates the colocalization of the stem of the DNA loop and the condensin, as seen in the yellow spot. (**C**) Model for DNA loop extrusion by condensin. Condensin (purple circle) anchors one strand of DNA and extrudes the other strand by a fast motor action.

Supplementary Materials for

Real-time imaging of DNA loop extrusion by condensin

Mahipal Ganji,[1] Indra A. Shaltiel,[2]* Shveta Bisht,[2]* Eugene Kim,[1] Ana Kalichava,[1]
Christian H. Haering,[2]† Cees Dekker[1]†

correspondence to: christian.haering@embl.de; c.dekker@tudelft.nl

This PDF file includes:

Materials and Methods
Figs S1 to S7
Captions for Movies S1 to S11

Other Supplementary Materials for this manuscript includes the following:

Movies S1 to S11

Materials and Methods

Preparation of biotin-labeled λ-DNA

The single-stranded DNA ends of lambda phage DNA (λ-DNA; D1521, Promega) were filled with DNA polymerase I large fragment (M0210, New England Biolabs), which lacks the exonuclease activity, in the presence of dTTP, dCTP, dGTP, and biotin-14-dATP (19524016, Invitrogen). The biotin-labelled DNA was then purified from excess nucleotides and polymerase using a PCR clean up kit (20021, Qiagen). This preparation produced DNA molecules of which the majority contained biotin moieties on both ends, as evidenced from the large fraction of DNA molecules that assembled as double tethers on the streptavidin-coated surfaces in our assay (Fig. S7). Note that molecules that did not incorporate biotin do not bind to the surface of the flow-cell, whereas molecules with a biotin moiety at only one of the two ends result in single-tethered DNAs that were ignored in the data analysis. The biotin-labelled DNA was stored at –20°C until use.

Condensin holocomplex purification

The pentameric *S. cerevisiae* condensin complex was purified as reported previously (*12*). Briefly, *S. cerevisiae* cells were transformed with a pair of 2μ-based high copy plasmids containing *TRP1 leu2-d pGAL10-YCS4 pGAL1-YCG1* and either *URA3 leu2-d pGAL7-SMC4-StrepII$_3$ pGAL10-SMC2 pGAL1-BRN1-His$_{12}$-HA$_3$* (wild-type, strain C4491) or *URA3 leu2-d pGAL7-smc4(Q302L)-StrepII$_3$ pGAL10-smc2(Q147L) pGAL1-BRN1-His$_{12}$-HA$_3$* (Q-loop ATPase mutant, strain C4724). Overexpression was induced by addition of galactose to 2% in –Trp −Ura media. Cell lysates were prepared in buffer A (50 mM TRIS-HCl pH 7.5, 200 mM NaCl, 5% (v/v) glycerol, 5 mM β-mercaptoethanol, 20 mM imidazole) supplemented with 1× cOmplete EDTA-free protease inhibitor mix (11873580001, Roche) in a FreezerMill (Spex), cleared by centrifugation, loaded onto a 5-mL HisTrap column (GE Healthcare) and eluted with 220 mM imidazole in buffer A. Eluate fractions were supplemented with 1 mM EDTA, 0.2 mM PMSF and 0.01% Tween-20, incubated overnight with Strep-Tactin Superflow high capacity resin (2-1208-010, IBA), and eluted with buffer B (50 mM TRIS-HCl pH 7.5, 200 mM NaCl, 5% (v/v) glycerol, 1 mM DTT) containing 10 mM desthiobiotin. After concentrating the eluate by ultrafiltration, final purification proceeded by size-exclusion chromatography with a Superose 6 column (GE Healthcare) pre-equilibrated in buffer B containing 1 mM $MgCl_2$ (Fig. S5). Purified protein was snap-frozen and stored at –80 °C until use.

ATPase assays

ATP hydrolysis assays (Fig. S5E) were performed as described (*12*). Reactions were set up in a volume of 10 μL, containing 0.5 μM condensin in 40 mM TRIS-HCl pH 7.5, 125 mM NaCl, 10 mM $MgCl_2$, 5% (v/v) glycerol and 1 mM DTT. Where indicated, 1 μg 6.4-kbp plasmid nicked with *Nb.Bbv*CI and purified by phenol-chloroform extraction followed by ethanol precipitation was included in the reaction. Reactions were initiated by addition of ATP to 5 mM (containing 6.7 nM [α-^{32}P]ATP) and incubated at room temperature. Every 180 s, for six consecutive time intervals, 1 μL of the reaction was spotted onto PEI cellulose F TLC plates (Merck), which were developed in 0.5 M LiCl and 1 M formic acid, exposed to imaging plates and analyzed on a Typhoon FLA9500 imager (GE Healthcare).

Fluorescent labeling of purified condensin complexes

A ybbR acceptor peptide sequence (GTDSLEFIASKLA; (*25*)) was introduced into the overexpression plasmid at the N terminus of Brn1, replacing amino acid residues 13–23 of the original protein (Fig. S5A). ybbR-tagged condensin complexes were purified as before from yeast cells (strain C5066) (Fig. S5B–D). The CoA-ATTO647N substrate for covalent coupling to the Serine hydroxyl group of the ybbR peptide was synthesized as described (*3*): 50 nmol of ATTO647N-maleimide (AD 647N-41, ATTO-TEC) were incubated at room temperature with 45.5 nmol Coenzyme A sodium salt hydrate (C3144, Sigma) in 0.1 mL of a 50:50 (v/v) mixture of DMSO:100 mM sodium phosphate pH 7.0 (aq; degassed). 15 minutes into the reaction, 100 nmol of tris(2-carboxyethyl)phosphine (646547, Sigma) were included and the reaction was terminated after one hour by addition of dithiothreitol to 330 nmol.

For the subsequent transfer of the ATTO647N-succinimidyl phosphopantetheine thioether moiety, purified condensin complexes (~5 μM) were incubated with a five-fold molar excess of CoA-ATTO647N in buffer B supplemented with 10 mM $MgCl_2$ and 1.2 μM *Sfp* phosphopantetheinyl transferase (P9302, New England Biolabs) for 16 hours at 6 ºC, shielded from light. After ultrafiltration, free dye and *Sfp* synthase were eliminated by size exclusion chromatography on a Superose 6 Increase column (GE Healthcare) pre-equilibrated in buffer B containing 1 mM $MgCl_2$. Peak fractions were pooled and concentrated by ultrafiltration. Fractions were analyzed by SDS-PAGE (NuPAGE 4-12% Bis-Tris gels, ThermoFisher) and fluorescence was detected on a Typhoon FLA9500 imager (GE Healthcare) with a 635-nm laser and a 665-nm long pass filter (Fig. S5).

Labeling efficiency was estimated to be 60-85% based on the absorbance ratio of 280 and 650 nm, using the calculated molar extinction coefficient of the condensin complex at 280 nm (335,670 M^{-1} cm^{-1}), the molar extinction coefficient of the ATTO647N dye at 650 nm (150,000 M^{-1} cm^{-1}) and correcting for the absorption at 280 nm by the dye ($\varepsilon_{280\ nm}/\varepsilon_{650\ nm}$ = 0.03).

Double-tethered DNA assay for single-molecule imaging

Microfluidic chambers were prepared using biotin-PEG/PEG-passivated quartz slides and cover slips as described previously (*15*). The volume of the flow cell was about 20 μL. The chambers were first incubated with 0.1 mg/mL streptavidin in T20 buffer (40 mM TRIS-HCl pH 7.5, 20 mM NaCl, 0.2 mM EDTA) for 1 min. Unbound streptavidin was washed off with 100 μL of T20 buffer. 35 μL of ~1 pM biotin-labelled DNA in T20 buffer was then introduced into the flow cell at a constant speed of 5 μL/min. Immediately thereafter, excess DNA was washed off with 100 μL of T20 buffer at the same flow rate. This preparation resulted in a sparse distribution of double-tethered DNA molecules that could be imaged individually. The surface-tethered DNA molecules were stained with 500 nM of Sytox Orange (S11368, ThermoFisher) in imaging buffer (50 mM TRIS-HCl pH 7.5, 50 mM NaCl, 2.5 mM $MgCl_2$, 1 mM DTT) and an oxygen scavenging system (5% (w/v) D-dextrose, 2 mM Trolox, 40 μg/mL glucose oxidase, 17 μg/mL catalase).

For imaging of SxO-stained DNA only, a 532-nm laser was used in a home-built epi-fluorescence microscope (*15*). In the case of dual-color imaging of SxO-stained DNA and ATTO647N-labelled condensin, a 532-nm laser was used in the epi-fluorescence mode to excite SxO (*15*), and a 640-nm laser was used through a quartz prism to create an

evanescent field for excitation of ATTO647N (*27*), respectively. This hybrid of epi and TIRF microscopy was optimal for co-imaging of DNA and condensin, as it allowed homogeneous illumination of SxO-stained DNA molecules in the epi-fluorescence mode while avoiding high fluorescence background resulting from free-floating labeled condensin molecules in the TIRF mode. The simultaneous imaging of λ-DNA and condensin was achieved by an alternating excitation scheme.

Image analysis and data processing

Fluorescence images were analysed using custom-built Matlab (Mathworks) software as described previously (*15*). Fluorescence intensity profiles of DNA molecules exhibiting loop structures were obtained by summing the intensity values from 11 pixels taken across a line perpendicular to the extended DNA in each frame. Background intensity was removed by 2d-median filtering. Subsequently, the intensities were normalized to the maximum value in order to correct for intensity fluctuations (such as bleaching) during the measurements. After obtaining the intensities for all frames, the normalized intensity profiles taken at subsequent time points were concatenated to build an intensity kymograph as shown in figures 3B, D, and E.

From the kymographs that were obtained from individual DNA molecules, the amount of DNA in the regions of I, II, and III (cf. Fig. 3C) was estimated as following. The position of the maximum fluorescence intensity at the looped DNA was used to determine the position of loop. To correct for the extended DNA beneath the loop, whose intensity needs to be subtracted for accurate determination of the loop size, the backbone DNA intensity, obtained by the median intensity of the pixels excluding a 11-pixel loop area, was subtracted. The size of the loop was determined by integrating the intensity from 11 pixels centred at the pixel with maximum intensity. The total intensity of DNA was determined ahead and behind the loop. Using the intensity information, the size of DNA (in kbp) in the loop, ahead, and behind the loop was obtained by normalization with the entire DNA intensity and multiplication by 48.5 kbp, i.e.:

$$DNA\ size\ in\ loop\ (bp) = \frac{\left(Int_{Loop} * 48{,}502\right)}{Total\ DNA\ intensity}$$

$$DNA\ ahead\ of\ loop\ (bp) = \frac{\left(Int_{ahead\ of\ loop} * 48{,}502\right)}{Total\ DNA\ intensity}$$

$$DNA\ behind\ of\ loop\ (bp) = \frac{\left(Int_{behind\ of\ loop} * 48{,}502\right)}{Total\ DNA\ intensity}$$

The DNA loop extrusion rate was determined in two ways: First, the rate was obtained from the slope of a simple linear fit to the linear rise in the first 15 seconds of data such as shown in figure 3G. The resulting data for the DNA loop extrusion rate are shown in figures 3I and J. In a second analysis, the nonlinear change of the loop extrusion rate versus time was considered. To extract the loop-extrusion rate in this regime, the time trace for the growth of DNA loop (e.g. Fig. 3C, red) was smoothed using the Savitzky-Golay method (2^{nd} polynomial order) with a moving window of 200 points. This was followed by taking

the first derivative between adjacent points, which yielded the extrusion rate in kbp/s at every time point. The result is a loop-extrusion rate that changes over time (see Fig. S4B for an example). Note that the rate drops quickly as loop growth proceeds.

For figure 3J, the relative extension of the DNA was obtained by dividing the observed end-to-end length of the DNA molecule by the contour length (20 μm for the full-length λ-DNA after 500nM SxO intercalation) of the piece of λ-DNA that is not contained in the loop. The DNA loop extrusion rate was then plotted against this relative extension in figure 3J.

For figure 3K, the force acting within the DNA was obtained from the relative extension of the DNA. The relative extension of DNA was converted to force via linear interpolation of the known force-extension curve that was experimentally obtained by single-molecule magnetic tweezer force spectroscopy (*15*). Note that the force exerted on DNA vs relative extension was independent of SxO concentration (*15*) and thus the known force-relative extension curve from Ganji and Kim *et al.* could simply be used to read off the forces from the experimental extension data. Figure 3K plots the loop extrusion rate as a function of the applied force thus calculated, for a number of individual molecules (N=6) that all exhibited stalling of the loop extrusion somewhere mid-molecule, i.e. where the DNA loop extrusion was not limited by reaching the end position of the DNA. The curve in figure 3K displays the average of the 6 curves from individual molecules (cf. Fig. S4E) for which the data are averaged across the common range of forces.

Supplementary figures

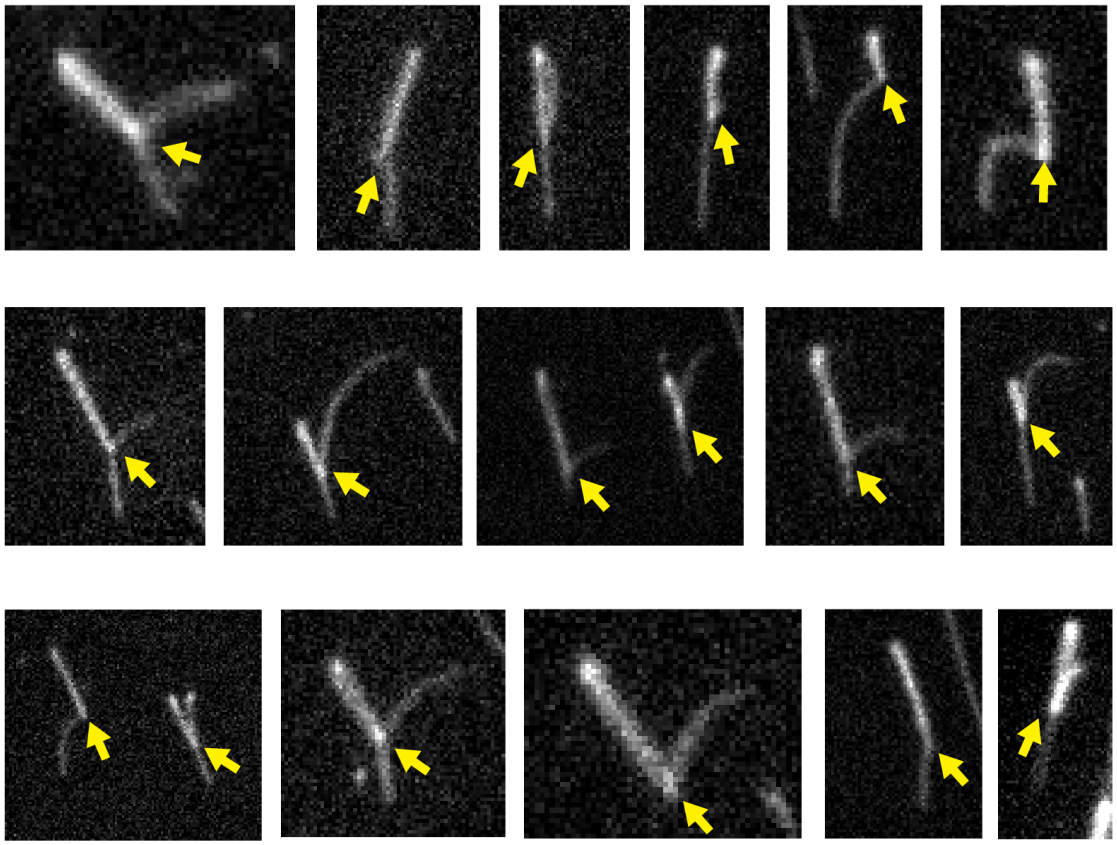

Fig. S1. Visualization of DNA loops that are induced by condensin and visualized by side-pulling through flow stretching. Each panel shows an individual double-tethered DNA molecule that is stained with SxO and that exhibits an extended loop. Yellow arrows indicate the bases of the loops.

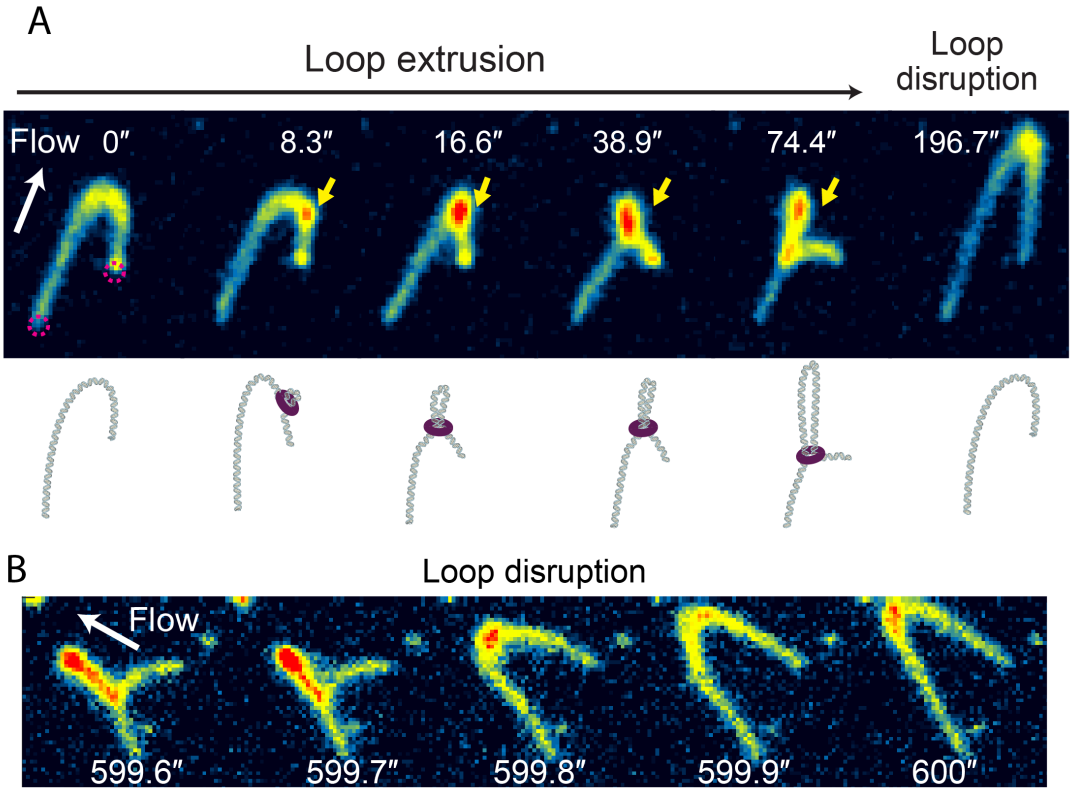

Fig. S2. (A) Movie snap-shots showing real-time DNA loop extrusion on double-tethered DNA, which was kept under constant flow. At time 8.3 seconds, a bright fluorescence density appeared (indicated by a yellow arrow) which grew over time until reaching a maximum size at 74 seconds. After 196.6 seconds, the loop suddenly disappeared, presumably due to dissociation of the condensin. (**B**) Snap-shots showing the instantaneous disruption of a loop that had been extruded by condensin. These snap-shots are extracted from the same movie as in figure 2A, right before the last snap-shot image shown there.

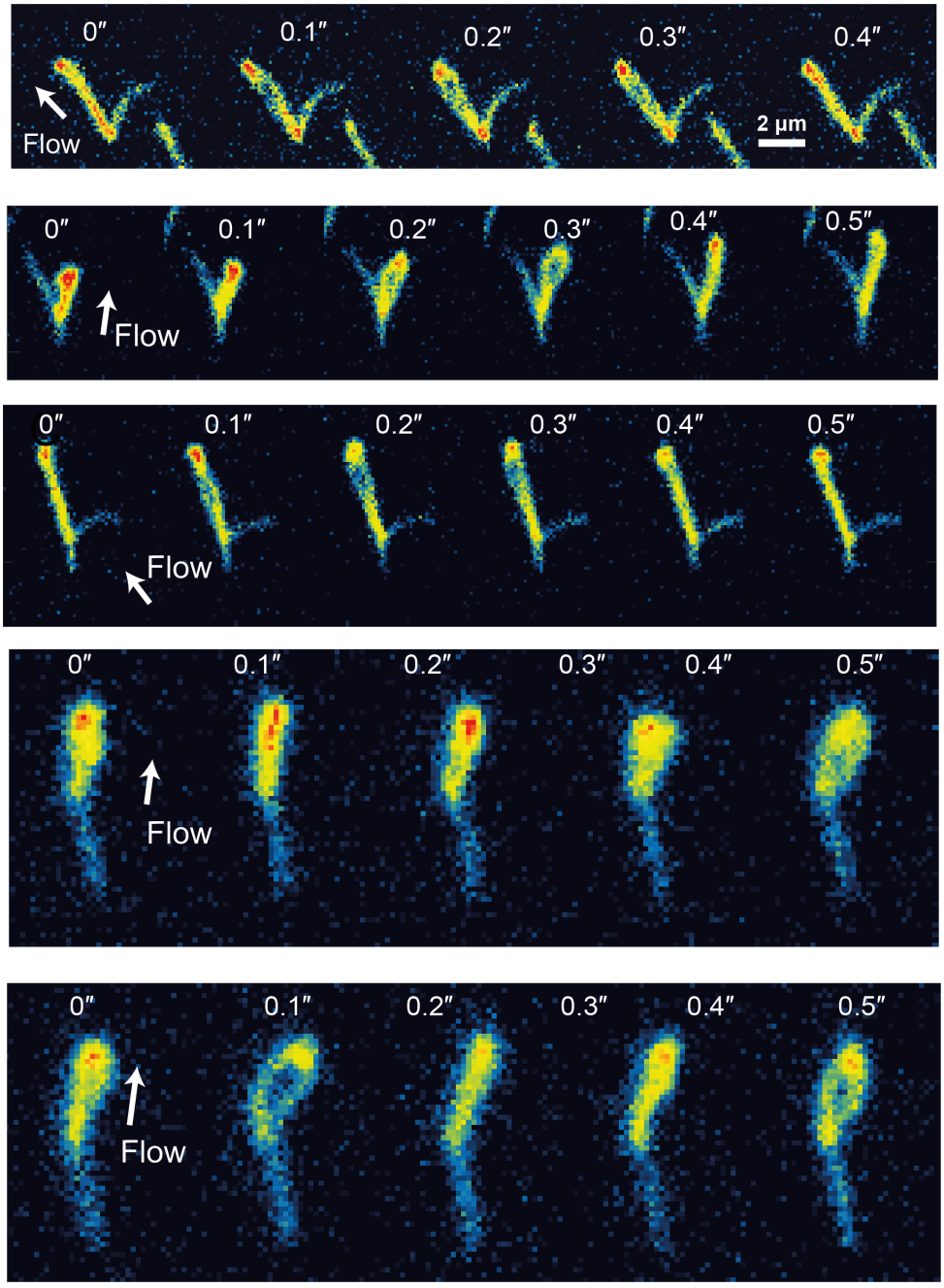

Fig. S3. Series of consecutive images showing spontaneous opening and closing of the DNA loop that was formed due to condensin activity, similar to data in figure 2B. Each horizontal panel shows a different DNA molecule.

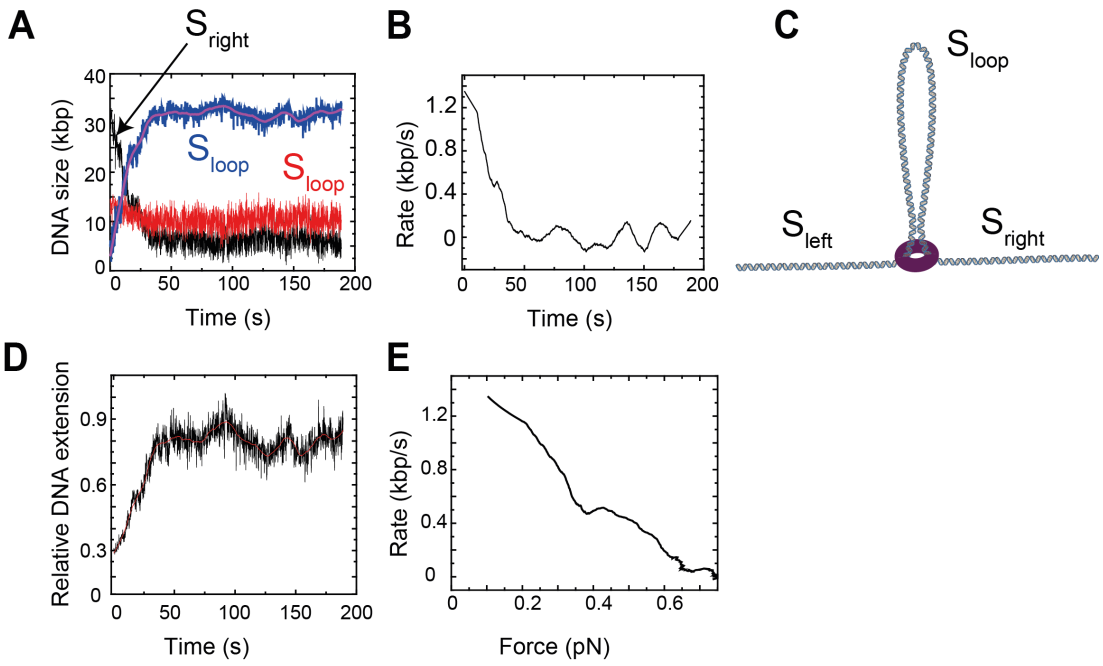

Fig. S4. Example of the extraction of the rate versus force plots. (**A**) The loop size in kbp, S_{loop} (blue), was first smoothened via Savitzy-Gollay filtering with 2nd order polynomial and 200 points (magenta line). (**B**) The rate of loop extrusion was then obtained from the first-order derivative of the adjacent points of the smoothened curve. (**C**) In order to obtain force values, the relative extension of DNA, defined as the end-to-end distance of the molecule (*L*) divided by the physical length of DNA that is not extruded in the loop, i.e. the length of S_{ahead} + S_{behind}, was extracted and smoothened, as shown in (**D**), followed by conversion to force via linear interpolation of the experimentally obtained force-extension curve (*15*). (**E**) As a result, the rate of loop extrusion was plotted against the force.

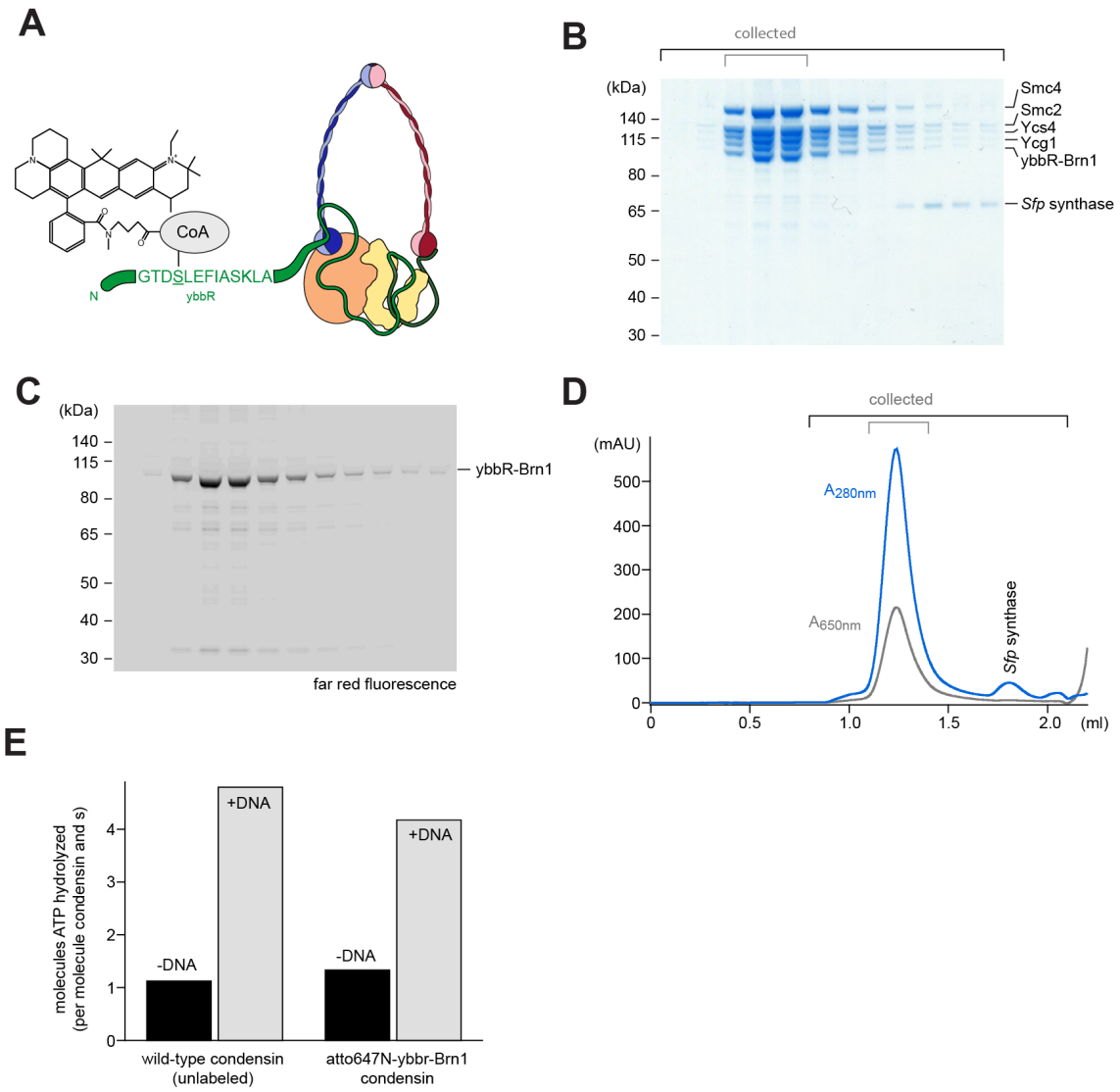

Fig. S5. Site-specific labeling of condensin with ATTO647N. (**A**) Purified condensin complexes harboring a ybbR tag on Brn1 were labeled with Coenzyme A-conjugated ATTO647N using *Sfp* synthase. (**B-D**) The reaction product was re-purified by size-exclusion chromatography and fractions resolved by SDS-PAGE and Coomassie Brilliant Blue staining (B) and in-gel detection of the ATTO647N fluorescence (C) of fractions of the corresponding size-exclusion chromatogram (D). (**E**) The catalytic integrity of the ATTO647N-labeled complex was confirmed by comparing the ATP hydrolysis activity to unlabeled wild-type condensin holocomplex in the presence and absence of DNA.

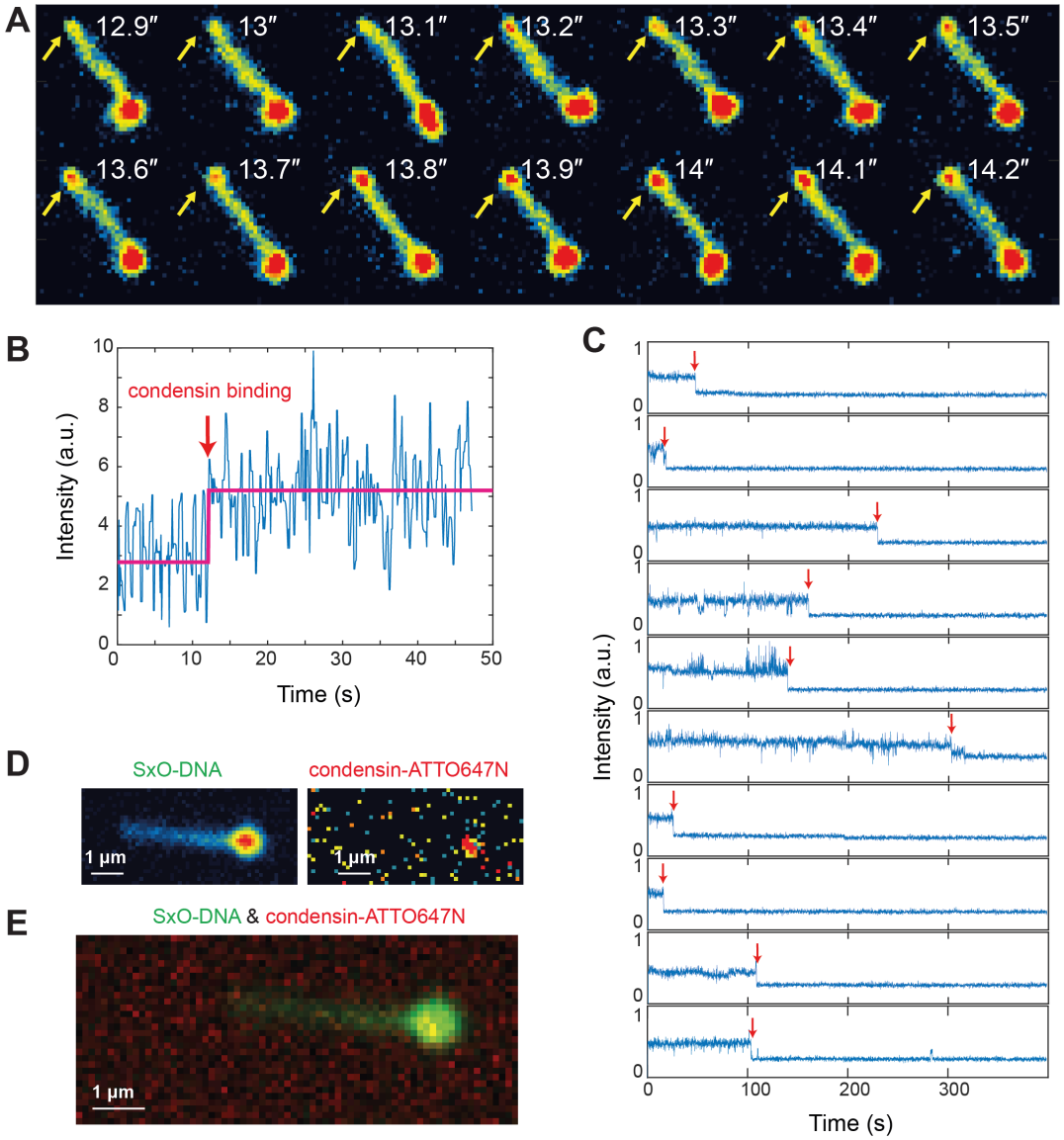

Fig. S6. Experimental data supporting that a single condensin unit induces DNA loop extrusion. **(A)** Series of snap-shots showing the initiation of DNA loop extrusion at the top end of the DNA, indicated by yellow arrows. At time point 13.2 s, a DNA loop is extruded. (**B**) The corresponding time trace of the fluorescence intensity collected from ATTO647N-labelled condensin at the location of the loop shown in (A). An abrupt increase in the fluorescence intensity is seen near time point 12 s, which indicates the binding of condensin. This coincides well with the appearance of the DNA loop at 13.2 s in panel A. (**C**) Time traces of fluorescence intensities of individual ATTO647N-labelled condensin complexes that are non-specifically bound to the surface of flow chambers. All the traces exhibit spontaneous single-step bleaching events, which proves that these complexes are present as monomers on the surface. (**D**) Fluorescence image of a SxO-stained DNA exhibiting an extruded loop (left) and an Atto647N-labelled condensin that is located at the stem of loop (right). (**E**) Overlaid images from panel (D). DNA is shown in green and condensin in red.

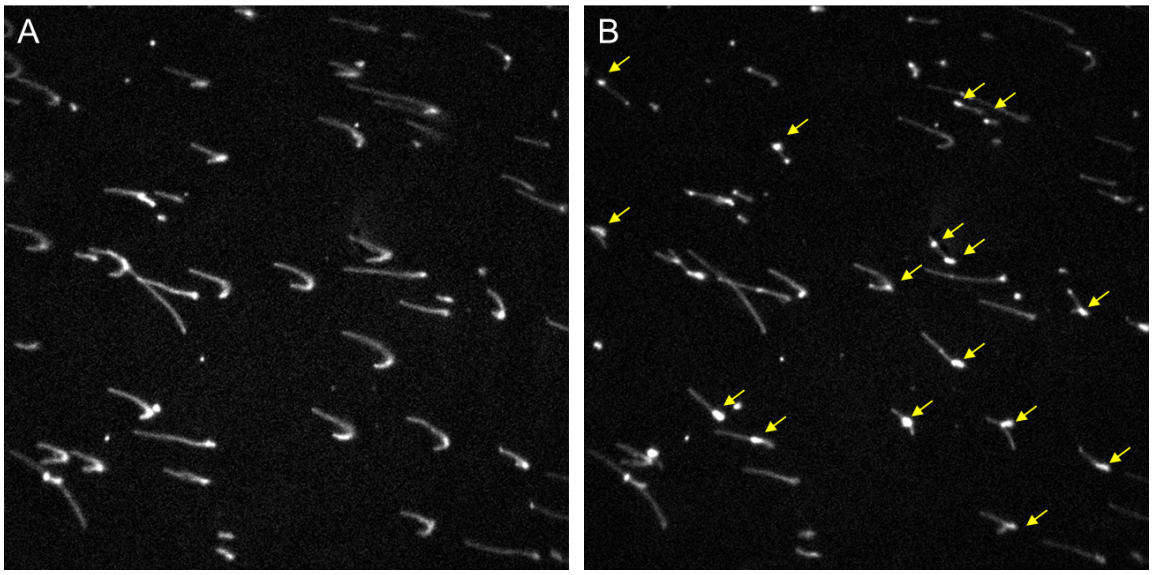

Fig. S7. Example of a field of view showing many SxO-labeled DNA molecules imaged in the fluorescence microscope in the presence of flow. These wide-field images show double-tethered DNA molecules before (**A**) and after (**B**) loop extrusion by condensin. Yellow arrows indicate extruded loops.

Supplementary movies legends

Movie S1. Movie showing SxO-stained double-tethered DNA in the absence of condensin, displaying a homogeneous fluorescence intensity.

Movie S2. Movie showing DNA compaction by condensin. Compaction can be identified as a bright fluorescence spot within the SxO-stained DNA.

Movie S3. Movie showing DNA that is compacted by condensin. Compaction can be identified as a bright fluorescence spot within the SxO-stained DNA. During this movie, a perpendicular flow was applied, which revealed that the bright spot as an extended DNA loop.

Movie S4-S5. Movies showing DNA loop extrusion on SxO-stained DNA under a constant flow. In both movies, DNA initially displays an inverted U-shape due to the applied flow. As the movies proceed, a bright fluorescence spot appears that grows into an extended loop, which finally stalls due to the increased force within the DNA. At its maximum size, the DNA molecule thus appears as an inverted Y-shape.

Movie S6-S7. Movies that show sudden single-step disruption of the DNA loops at the end of movies S4-S5, presumably due to dissociation of the condensin complexes that had created the loop.

Movie S8. Movie that starts condensin-mediated DNA compaction under constant flow perpendicular to DNA. Near the end of the movie the DNA loop breaks, most likely due to a photo-induced double stranded break. This rare event nicely shows the two DNA strands that form the extruded loop.

Movies S9-S10. Movies of DNA loop extrusion on double-tethered DNA in the absence of flow. The DNA initially exhibits a homogenous fluorescence intensity along its length. As time progresses, a bright fluorescence spot appears that migrates towards one of the two ends of the attached DNA.

Movie S11. Movie with overlaid channels of fluorescence from SxO-stained DNA (green) and ATTO647N-labeled condensin (red), showing the presence of condensin at the stem of the extruded DNA loop. A constant flow under an angle with the DNA shows the extended DNA loop. Towards the end of the movie, flow was stopped, which resulted in a bright spot on the stretched DNA. Figures 4A and B were extracted from this movie.